Experimental dynamics of an annulus of vorticity in a pure electron plasma

A. J. Peurrung and J. Fajans
Department of Physics, University of California, Berkeley, Berkeley, California 94720

(Received 23 June 1992; accepted 16 October 1992)

The dynamics of hollow, cylindrically shaped pure electron plasmas are studied. Since these plasmas behave like two-dimensional (2-D) fluids with low viscosity, their evolution parallels the evolution of 2-D fluid vorticity annuli inside frictionless circular containers. Growth of the Kelvin–Helmholtz instability in circular geometry is observed. The formation and subsequent interaction of vortices are studied as a function of ring thickness. Small initial perturbations can dramatically increase the symmetry and repeatability of the dynamics.

I. INTRODUCTION

Fluid shear layers are susceptible to the Kelvin–Helmholtz instability. This instability quickly leads to vortex formation and can eventually lead to two-dimensional (2-D) turbulence.[1,2] The instability is observable in many systems including oceans[3] and planetary atmospheres.[4,5] Hollow non-neutral plasmas and charged particle beams are susceptible to an analogous instability called the diocotron instability.[6] Because non-neutral plasmas have very low viscosity and are easy to control, we study here the Kelvin–Helmholtz/diocotron instability in a pure electron plasma.

The equations governing inviscid, incompressible, 2-D fluids are isomorphic to the equations governing ideal, magnetized, pure electron plasmas, consequently, the fluid and plasma systems evolve identically.[6,7] The dynamical variables are interpreted differently; the fluid vorticity, ω, maps to the scaled density, $4\pi en/cB$, where n is the plasma density, $B\hat{\mathbf{z}}$ is the magnetic field, e is the electron's charge, and c is the speed of light. The streamfunction, ψ, maps to the scaled electric potential, $\phi(x,y)/eB$, where $(x\hat{\mathbf{x}}+y\hat{\mathbf{y}})$ defines the radial vector perpendicular to the magnetic field. The fluid streamfunction equation $\nabla^2\psi=-\omega$ maps to the Poisson equation, $\nabla^2\phi=-4\pi en$, and the fluid velocity equation

$$\mathbf{v}(x,y)=\left(\frac{\partial\psi}{\partial y}\hat{x}-\frac{\partial\psi}{\partial x}\hat{y}\right), \tag{1}$$

maps to the plasma $\mathbf{E}\times\mathbf{B}$ drift equation,

$$\mathbf{v}(x,y)=\frac{1}{cB}\left(\frac{\partial\phi}{\partial y}\hat{x}-\frac{\partial\phi}{\partial x}\hat{y}\right). \tag{2}$$

Viscous fluid flow is subject to no-slip wall boundary conditions. Plasma flow, however, is allowed to be nonzero even at the wall boundary. Due to the exceptionally low viscosity of the plasma, the dynamics is nearly inviscid and we can follow the dynamical evolution to much later times than is possible in conventional fluid experiments.[8]

This experiment exploits the mapping between fluid vorticity and plasma density. Although fluid vorticity is the fundamental quantity in fluid dynamics,[9,10] experimental studies are hampered by the fact that fluid velocity, not vorticity, is the quantity most readily controlled and measured. In plasma experiments, density is the quantity most easily manipulated and measured. Our hollow electron plasma rings correspond to a vorticity annulus in an otherwise irrotational, incompressible, inviscid, circularly bounded fluid. The instability that exists for this state has been observed in many experimental devices.[11–15] Our ability to both extensively control the plasma's initial shape and clearly image its evolution make possible the more detailed study presented here.

Figure 1 shows the experimental geometry. The plasma is trapped inside a series of gate cylinders that are individually biased to provide axial confinement. Radial confinement is assured by an axial magnetic field. Normally, the plasma is held in a central, grounded gate while a large negative voltage is applied to two endgates. During plasma injection, the left endgate is raised to ground, allowing plasma to stream into the confinement region from a thermionically emitting, tungsten-wire filament. The plasma is hollowed by raising one endgate part of the way toward ground. Since the center of the plasma has the most negative potential, the center escapes through the lowered potential barrier. The ring thickness is controlled by setting the gate potential;[15] thinner rings are produced by bringing the gate closer to ground. Images are obtained by grounding the right endgate, thereby allowing the plasma to stream out along the magnetic field lines. The plasma then strikes a phosphor screen, producing a visible image. The time required for imaging is much shorter than all dynamical time scales.

Plasmas in this experiment have a density of approximately 1.0×10^8 cm^{-3}, and a temperature of approximately 2 eV. The plasma is short; the length is somewhat less than 3.5 cm and exhibits a slight dependence on density. The diameter of the confining gates is 1.905 cm, and the outer radius of the plasmas used throughout this experiment is approximately 1.1 cm. The ring's radial profile is rounded and the inside and the outside edge profiles are not necessarily identical. The maximum vorticity is a slight function of ring thickness for the thicker rings but declines substantially for the thinnest rings.

The fluid analogy rests on two basic physical assumptions. The first is that the end-to-end bounce time of electrons in the plasma is much shorter than all other evolution time scales. Since gyromotion plays no role in the

 0899-8213/93/020493-07$06.00 © 1993 American Institute of Physics

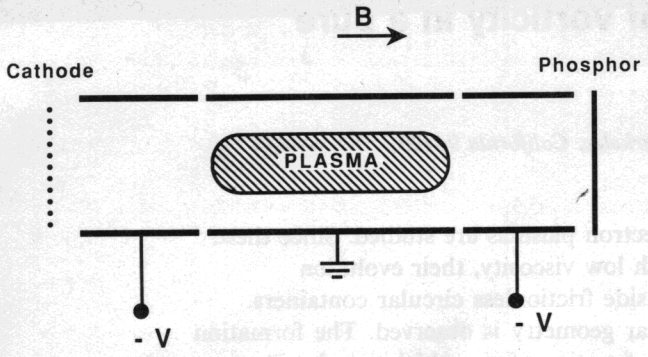

FIG. 1. Trap geometry.

dynamics of a strongly magnetized plasma, this assumption is generally true. The rapid electron bounce motion causes the plasma to act as if it is "averaged" along the axial dimension, rendering it effectively two-dimensional. The second assumption is that only $\mathbf{E}\times\mathbf{B}$ drift dynamics govern the two-dimensional motion of the plasma. This "zero viscosity" assumption is certainly true at early times, but is eventually broken by slower types of plasma transport. Since both the electron–electron collision time (1–10 msec) and the electron–neutral gas molecule collision time (>100 msec) are considerably longer than the instability time, these effects are unimportant. Energy-dependent drift arising in the plasma edge region may be the dominant type of transport which breaks the fluid analogy.[16]

Initial perturbations were not used in these experiments except as described in Sec. IV. This allows the instability to grow from the wide spectrum of naturally occurring noise. Thus, the observed mode corresponds to the fastest growing unstable mode for a particular initial geometry.

II. EARLY DYNAMICS

The initial plasma evolution is dominated by velocity shear, which quickly leads to the Kelvin–Helmholtz instability. The three image pairs in Fig. 2 show annular plasmas before and after the onset of instability. Although many modes are often unstable, a fastest growing mode with an integer l wavelengths around the annulus soon grows to dominate the dynamics. This mode number l is a function of the ring geometry; thinner rings have higher l values. Figure 3 contains images of plasmas with a variety of mode numbers. Figure 4 shows both the observed and theoretically expected[6,17–20] mode numbers as a function of ring geometry. We believe that the discrepancy between the observed and predicted mode number for very thin rings is due to finite length effects. This and other problems with the fluid analogy are discussed later.

The Kelvin–Helmholtz instability deforms the shear layer boundary, as is shown in Fig. 5 for one wavelength of an evolving $\ell=4$ mode plasma. We also show the deformation predicted by Michalke's linearized model of instability growth for a hyperbolic tangent velocity profile.[21] For both theory and experiment, the shear boundary is assumed to be that point where the vorticity has fallen by

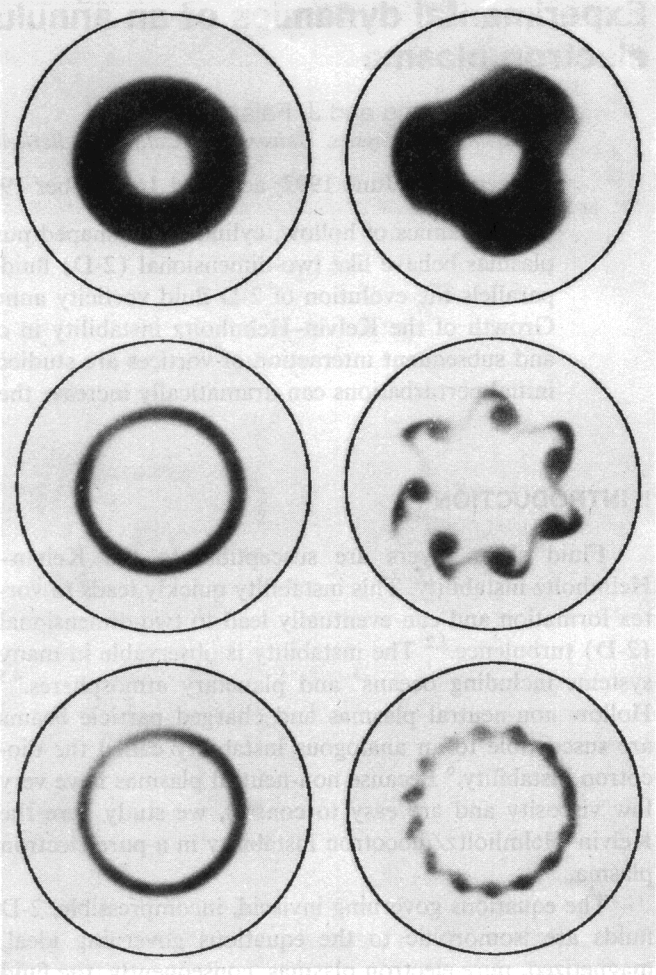

FIG. 2. Images of annular plasmas for three different thicknesses (0.67, 0.17, and 0.14 cm). The left column is at $t=0$. The right is after the onset of the Kelvin–Helmholtz instability. The outer circle indicates the conducting wall. The density scaling has been individually adjusted for maximum contrast.

half, and the amplitude and phase of the theoretical curve is adjusted for best fit.

The deformations on the outer boundary lag the deformations on the inner boundary (see Fig. 5). Inviscid fluid theory predicts that the fastest growing mode for a thin ring with a hard-edged vorticity profile far from the wall has a phase lag of 115.2°. A linear shear layer with a hyperbolic tangent profile has a phase lag of approximately 107°.[21] Except for those with $l=3$, all of our plasmas have a phase lag between 105° and 111°. For very thick rings, the circular nature of the geometry may have a significant effect.

By comparing successive plasma images we can measure the instability growth rate. The amplitude of the instability is defined to be the amount of deformation in the annular shape, and is measured by Fourier analyzing the edges of the plasma. Since the imaging process is destructive, we must recreate the plasma for each image. Because deliberate initial seeding predetermines the mode number, we allow the instability to grow from the noise. Clearly the successive plasmas need to be nearly identical for our tech-

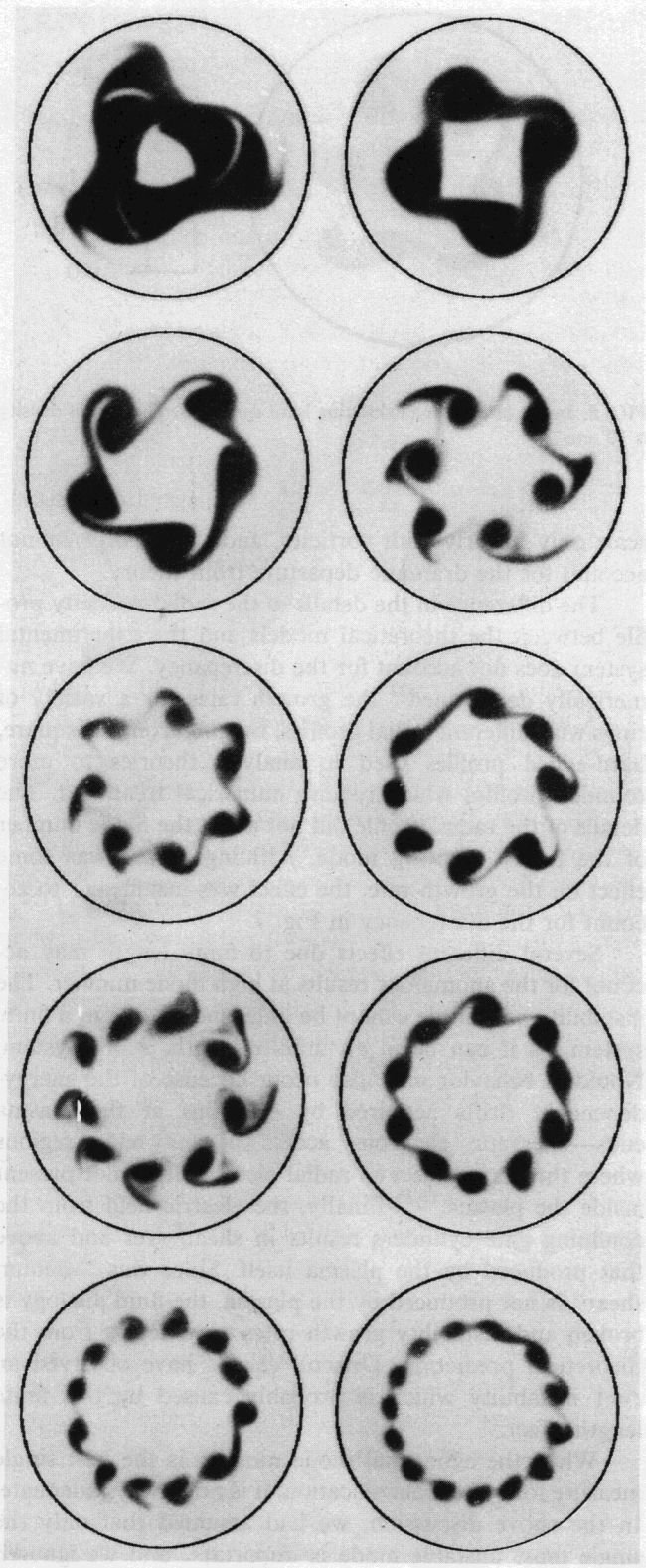

FIG. 3. Images of unstable plasmas with a variety of mode numbers. The density scaling has been individually adjusted for maximum contrast.

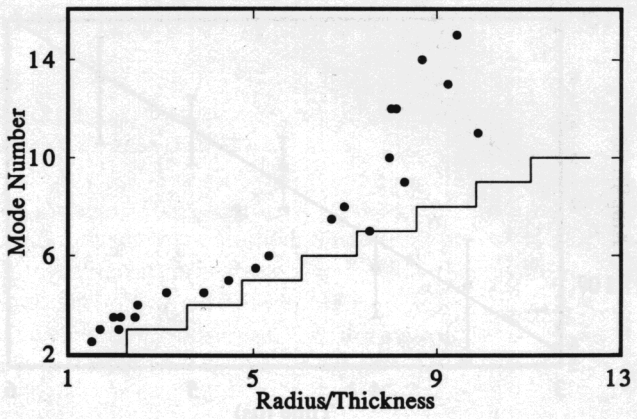

FIG. 4. Fastest growing mode versus ring thickness. The outer radius is held constant at 1.25 cm. Experimental observations (points) and predictions from the inviscid shear layer model (solid staircase) are shown. Half-integer wave numbers indicate that the system is able to grow in either of two modes.

nique to work. Figure 6 shows the instability growth for a $l=4$ plasma. To reduce shot-to-shot noise, the results from many images are averaged at each time.

As shown in Fig. 6, the instability growth is rapid and approximately exponential. The real part of the frequency is 6.3×10^6 rad/sec (one full revolution in 4.0 μsec), and the ratio between the imaginary and real parts of frequency is $\omega_i{:}\omega_r = 1{:}6$. This growth rate is roughly half the rate predicted by numerical simulations of smooth profile rings. Other experiments have also observed poor agreement with predicted growth rates.[7,15]

Equation (2) predicts that plasma velocities and shears are inversely proportional to magnetic field strength. Most of our measurements are taken at our highest possible magnetic field ($B=2$ kG), but we also studied the behavior of the higher shears obtainable at lower field strength. Although the data are less accurate because the frequencies are higher, both the real and imaginary parts of frequency appear to scale properly with shear. The fastest growing mode number is clearly independent of the shear magnitude. This agreement between hollow plasma behavior and an inviscid fluid model was also found by Rosenthal *et al.*[14] They found that mode number and growth rate scale properly with the plasma density, the

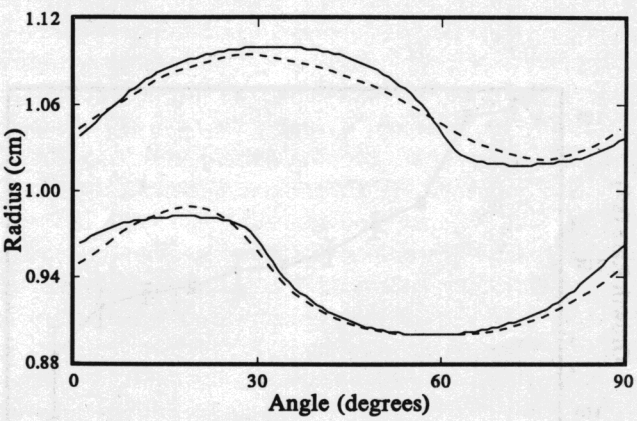

FIG. 5. The observed (dashed) and predicted (solid) shape of an evolving $\ell=4$ plasma. The lines indicate the contour where the vorticity has fallen to half of its maximum value. The angle is measured azimuthally around the ring.

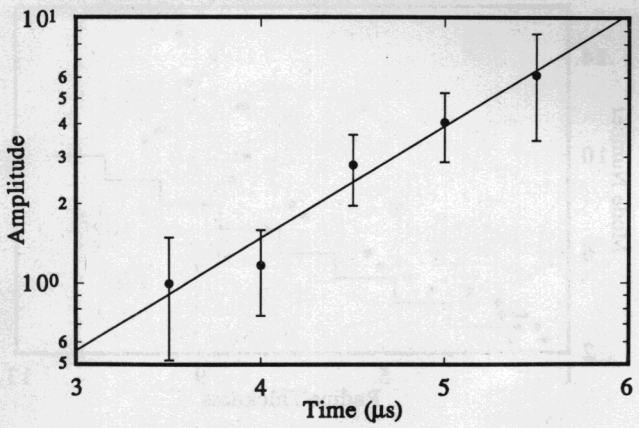

FIG. 6. Amplitude of $\ell=4$ instability versus time. Before $t=3.5$ μsec the dominant mode is not distinguishable. After $t=5.5$ μsec the mode is clearly nonlinear. The amplitude is measured in arbitrary units.

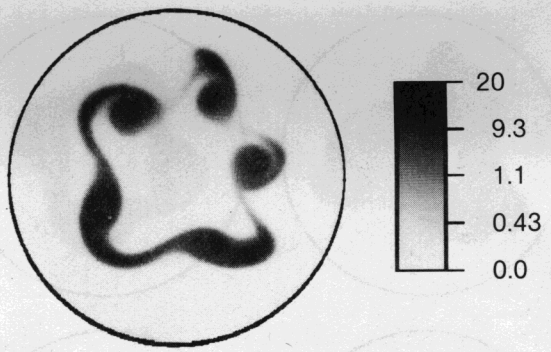

FIG. 8. Image of a plasma exhibiting local dynamics. The unit of density is 10^7 cm^{-3}.

magnetic field, and the shear from a central vortex. In their experiment, a voltage applied to a central conductor inside the hollow plasma mimics the effect of a compact central vortex inside the plasma.

The frequencies and growth rates for the fastest growing mode of a planar Kelvin–Helmholtz instability are independent of changes in the shear layer thickness which maintain constant vorticity. Such changes merely change the instability wave number. Consequently, we would expect that as the thickness of an annular shear layer becomes small compared with its radius, the growth rate should approach a limiting value equal to the growth rate of a straightened shear layer in linear geometry. This prediction is not born out by experimental observation. Figure 7 shows the measured growth rate as a function of mode number. Systems with a clearly dominant, fastest growing mode were selected by varying the annular thickness as in Fig. 4. The growth rate monotonically decreases with mode number, showing a large drop after $\ell=4$. Above $\ell\approx 14$ the instability vanishes entirely. While the maximum vorticity is a slight function of ring thickness, growth rates

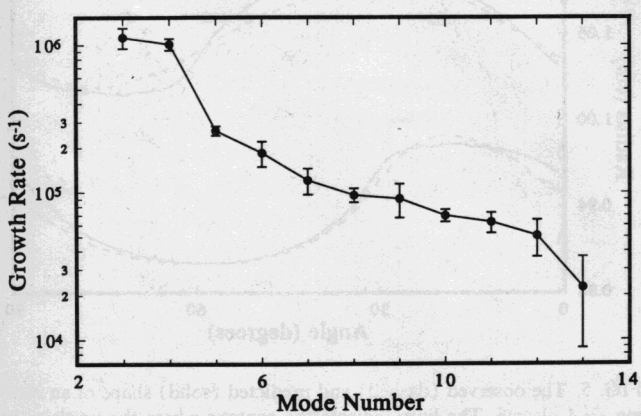

FIG. 7. Instability growth rate versus mode number. Beyond mode number 14 the system is stable.

scale only linearly with vorticity, and this change cannot account for the dramatic departure from theory.

The difference in the details of the radial vorticity profile between the theoretical models and the experimental system does not account for the discrepancy. We have numerically determined[22] the growth rates for a variety of rings with different radial profiles, ranging from the square, hard-edged profiles used in analytic theories to more rounded profiles which require numerical treatment. The details of the radial profile did not affect the mode number of the fastest growing mode. Although there was some effect on the growth rate, the effect was insufficient to account for the discrepancy in Fig. 7.

Several different effects due to finite length may account for the anomalous results at high mode number. The instability amplitude cannot be independent of z in a finite system, as it can be in an infinite length, $k_z=0$ system. Nonideal behavior may also occur because of the energy-dependent drifts acquired by electrons at the plasma ends—energetic electrons access plasma edge regions where they are subject to radial electric fields not present inside the plasma.[16,23] Finally, the electric field from the confining gate cylinders results in shear over and above that produced by the plasma itself. Since this "vacuum shear" is not produced by the plasma, the fluid analogy is broken and instability growth rates may depart from the theoretical prediction. Driscoll *et al.*[15] have observed an $\ell=1$ instability which is probably caused by this finite length effect.[24]

While the azimuthal mode number is the best single measure for system classification, it is not always adequate. In the above discussion, we had assumed that only the single most unstable mode is important, and we ignored any other unstable modes. Experimentally, the single mode description often fails. Because of the high growth rate, the dynamics are largely local; different sections of the ring initially develop independently. For example, in Fig. 8, the right side has a smaller wavelength and is more developed; fluid theory for the corresponding planar shear layer predicts that the fastest growing wavelength fits $4\frac{1}{2}$ times around the ring circumference and diocotron theory predicts that the $l=4$ and 5 modes are equally unstable. Although such local behavior is common, we can usually

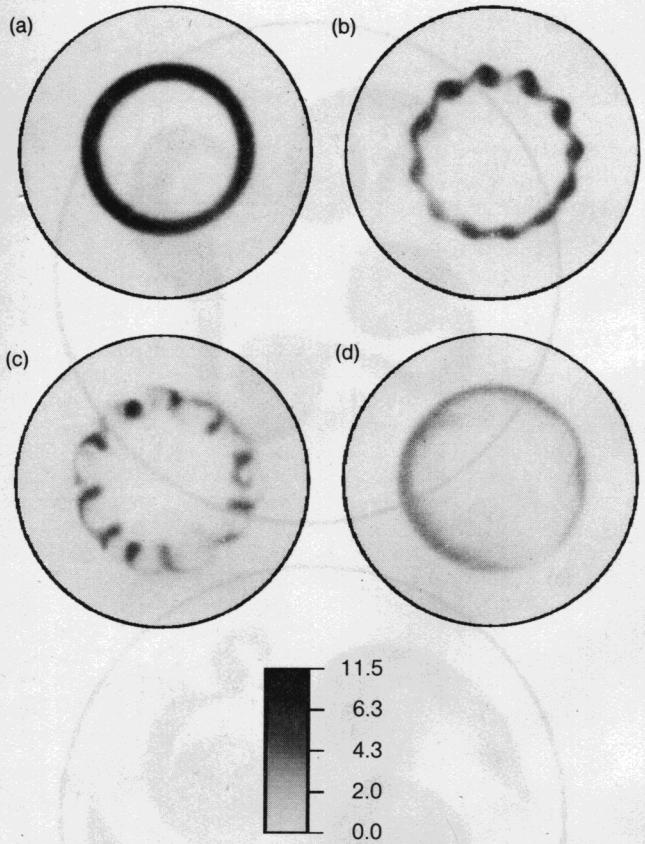

FIG. 9. Four images at different times (0, 100, 140, and 380 μsec) in the development of a mode number 12 plasma. The unit of density is 10^6 cm^{-3}.

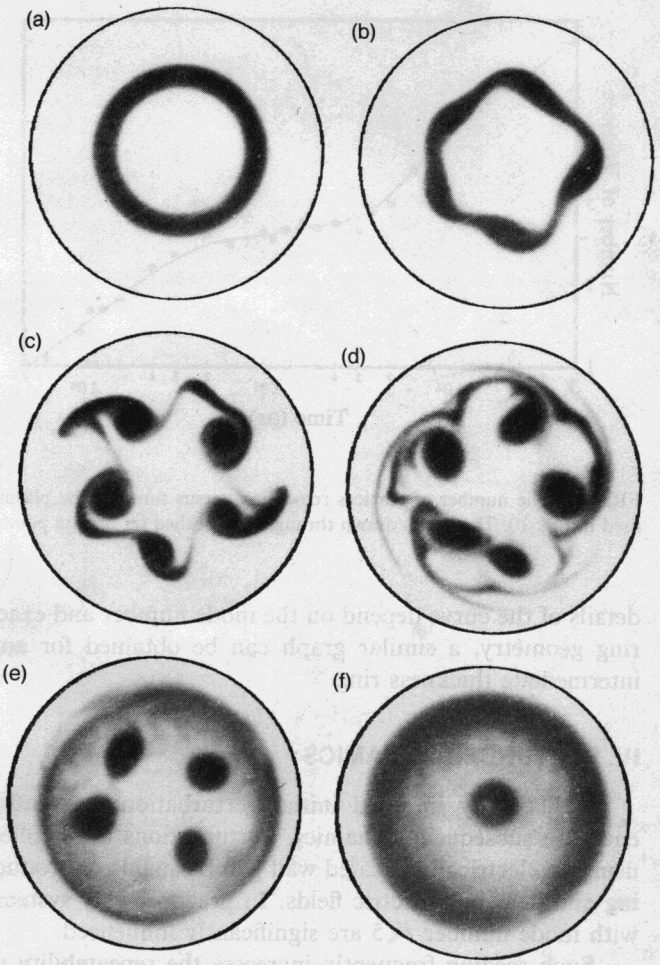

FIG. 10. Six images at different times (0, 16, 22, 32, 160, and 1500 μsec) in the development of a mode number 5 plasma. The density scaling is the same as that in Fig. 8.

obtain a single dominant mode by correctly tuning the ring thickness.

III. LATE DYNAMICS

Thick, thin, and intermediate rings evolve differently at late times. Vortex formation occurs as a result of the Kelvin–Helmholtz instability,[25–28] and the fate of these vortices distinguishes these three types of evolution. In thick ring systems, with mode numbers 3 or 4, the vortices merge even as they are being formed because the vortices are large and are formed close together.[29,30] In a thin ring system ($\ell > 10$), on the other hand, many small and well-separated vortices are formed. As shown in Fig. 9, these vortices subsequently disperse and smear out, leaving a broader annulus which does not evolve further. Thin ring behavior is not surprising in light of the increasing importance of finite length effects for thin rings. The apparent nonconservation of brightness in this figure actually results from the strongly nonlinear dependence of image brightness on plasma density.

Intermediate thickness ring evolution is the most involved and long lasting. Figure 10 shows six images at different times in the evolution of an $\ell = 5$ plasma. In these systems, which occur for $5 < \ell < 9$, the instability leads to the formation of ℓ-independent, interacting vortices.[7] These vortices then interact and merge on a time scale 10 to 100 times longer than the Kelvin–Helmholtz growth time scale. Figures 10(a) and 10(b) show the initial and exponentially growing states of the system. Figure 10(c) shows the system when the vortex formation is complete. By Fig. 10(d), the vortices are interacting both with each other and with the parts of the ring that were not incorporated into a vortex. These ring remnants are stretched and convected until they form a diffuse background vorticity. At this time two of the initial vortices are about to merge. In Fig. 10(e) only four vortices remain, two of which are interacting strongly and will shortly merge. The interaction proceeds until only one central vortex remains, as shown in Fig. 10(f). Any further change in the plasma profile involves slow cross-field transport within the plasma and is not of interest here. That one central vortex is the final state in a system with only one sign of vorticity has been anticipated by numerical simulations.[2,31] Due to the very long time over which these systems evolve, the unavoidable small initial variations have a large effect on the late dynamics. Any study of this vortex interaction and merger process is necessarily statistical. Figure 11 shows the average number of vortices remaining as a function of time for the initial conditions used in Fig. 10. Although the

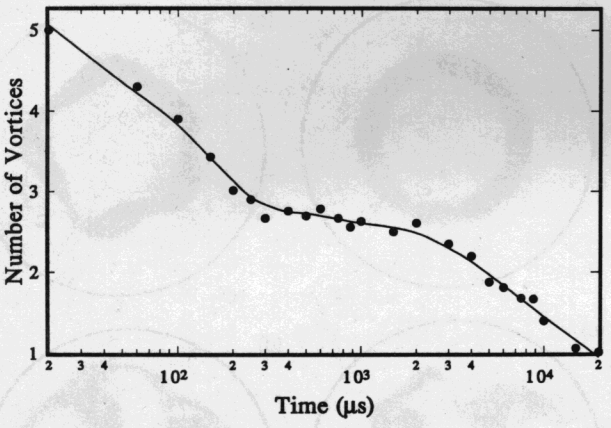

FIG. 11. The number of vortices remaining versus time for the plasma used in Fig. 10. The line is drawn through a smoothed set of data points.

details of the curve depend on the mode number and exact ring geometry, a similar graph can be obtained for any intermediate thickness ring.

IV. PERTURBED DYNAMICS

Deliberately imposed initial perturbations can influence the subsequent dynamics. Perturbations are applied using an electrically isolated wall patch capable of producing and detecting electric fields. In practice, only systems with mode number $\ell \ll 5$ are significantly influenced.

Such seeding frequently increases the repeatability of the dynamics without greatly influencing their general form. Often the development proceeds more quickly. More dramatic, however, is the symmetry enhancement produced by certain initial perturbations. Figure 12 shows the same system with and without an imposed perturbation. As Fig. 12(a) demonstrates, the unseeded system normally has mode number $\ell=4$, but does not have especially high symmetry. The seeded plasma [Fig. 12(b)] is more evolved, and yet retains the global inversion symmetry, $(x,y) \rightarrow (-x,-y)$. Seeded plasmas often retain their symmetry to quite late times, delaying the onset of vortex merger. An appropriate perturbation can also change the observed mode number by ± 1. For example, a system that normally has $\ell=5$ can be seeded to produce four larger vortices.

V. CONCLUSION

A hollow, magnetized, pure electron plasma behaves like a circular shear layer in an inviscid, incompressible, 2-D fluid. Our ability to directly manipulate and measure the "vorticity" of this low-viscosity electron fluid allows us to study long term dynamics for a variety of initial conditions. Modeling the system as a fluid shear layer accurately predicts the shape of the evolving instability but fails to accurately predict the growth rates. At late times, three different outcomes are observed for thin, thick, and intermediate rings. Finally, certain initial perturbations result in a persistent high degree of symmetry.

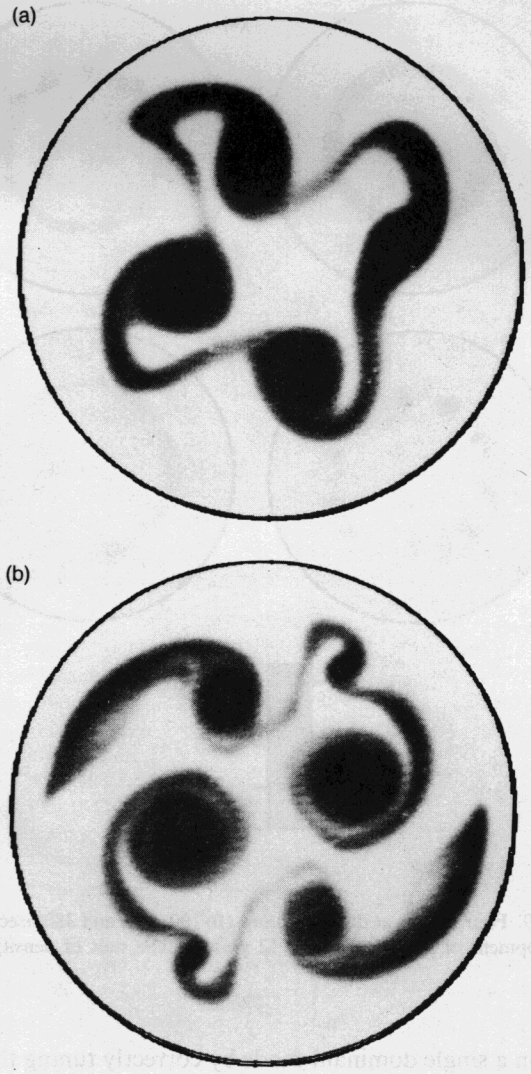

FIG. 12. Two images of initially identical plasmas without (a) and with (b) a symmetry enhancing perturbation. The density scaling is the same as that in Fig. 8.

ACKNOWLEDGMENTS

We thank Dr. Ralph Smith of the University of California, San Diego for his helpful comments and for the computer software used to predict the instability growth rates for smooth profiles.

This work is supported by the Office of Naval Research and by the National Science Foundation.

[1] M. Lesieur, C. Staquet, P. Le Roy, and P. Conte, "The mixing layer and its coherence examined from the point of view of two-dimensional turbulence," J. Fluid Mech. **192**, 511 (1988).
[2] P. S. Marcus, "Vortex dynamics in a shearing zonal flow," J. Fluid Mech. **215**, 393 (1990).
[3] M. E. Stern, "Evolution of locally unstable shear flow near a wall or a coast," J. Fluid Mech. **198**, 79 (1989).
[4] N. B. Ward, "The exploration of certain features of tornado dynamics using a laboratory model," J. Atmos. Sci. **29**, 1194 (1972).
[5] J. Sommeria, S. D. Meyers, and H. L. Swinney, "Laboratory simulation of Jupiter's Great Red Spot," Nature **331**, 689 (1988).
[6] R. H. Levy, "Diocotron instability in a cylindrical geometry," Phys. Fluids **8**, 1288 (1965).
[7] G. B. Rosenthal, "Epxerimental studies of an annular nonneutral elec-

tron plasma," Ph.D. thesis, University of California, Los Angeles, 1990.
[8]J. R. Weske and T. M. Rankin, "Generation of secondary motions in the field of a vortex," Phys. Fluids **6**, 1397 (1963).
[9]C. C. Lin, *Theory of Hydro-Dynamic Stability* (Cambridge U.P., London, 1966).
[10]J.-L. Balint and J. M. Wallace, "The statistical properties of the vorticity field of a two-stream mixing layer," in *Advances in Turbulence 2*, edited by H. H. Fernholz and H. E. Fiedler (Springer-Verlag, Heidelberg, 1989), p. 74.
[11]R. L. Kyhl and H. F. Webster, "Breakup of hollow cylindrical electron beams," IRE Trans. Electron Devices **3**, 172 (1956).
[12]C. A. Kapetanakos, D. A. Hammer, and C. D. Striffler, "Destructive instabilities in hollow intense relativistic electron beams," Phys. Rev. Lett. **30**, 1303 (1973).
[13]Y. Carmel and J. A. Nation, "Instability of an unneutralized relativistic electron beam," Phys. Rev. Lett. **31**, 286 (1973).
[14]G. Rosenthal, G. Dimonte, and A. Y. Wong, "Stabilization of diocotron instability in an annular plasma," Phys. Fluids **30**, 3257 (1987).
[15]C. F. Driscoll and K. S. Fine, "Experiments on vortex dynamics in pure electron plasmas," Phys. Fluids B **2**, 1359 (1990).
[16]A. J. Peurrung, "Imaging of instabilities in a pure electron plasma," Ph.D. thesis, University of California, Berkeley, 1992.
[17]R. W. Gould, "A field analysis of an M type backward oscillator," Ph.D. thesis, California Institute of Technology, 1956.
[18]A. Michalke and A. Timme, "On the inviscid instability of certain two-dimensional vortex-type flows," J. Fluid Mech. **29**, 647 (1967).
[19]F. H. Busse, "Shear flow instabilities in rotation systems," J. Fluid Mech. **33**, 577 (1968).
[20]R. Rotunno, "A note on the stability of a cylindrical vortex sheet," J. Fluid Mech. **87**, 761 (1978).
[21]A. Michalke, "On the inviscid instability of the hyperbolic-tangent velocity profile," J. Fluid Mech. **19**, 543 (1964).
[22]Software provided by Ralph Smith, University of California, San Diego.
[23]A. J. Peurrung and J. Fajans, "Non-neutral plasma shapes and edge profiles," Phys. Fluids B **2**, 693 (1990).
[24]R. A. Smith, "Effects of electrostatic confinement fields and finite gyroradius on an instability on hollow electron columns," Phys. Fluids B **4**, 287 (1992).
[25]A. Michalke, "Vortex formation in a free boundary layer according to stability theory," J. Fluid Mech. **22**, 371 (1965).
[26]R. H. Levy and R. W. Hockney, "Computer experiments on low-density, crossed-field electron beams," Phys. Fluids **11**, 766 (1968).
[27]H. S. Husain and F. Hussain, "Subharmonic resonance in a shear layer," in Ref. 10, p. 96.
[28]E. Panides and R. Chevray, "Vortex dynamics in a plane, moderate-Reynolds-number shear layer," J. Fluid Mech. **214**, 411 (1990).
[29]M. V. Melander, N. J. Zabusky, and J. C. McWilliams, "Axisymmetrization and vorticity-gradient intensification of an isolated two-dimensional vortex through filamentation," J. Fluid Mech. **195**, 303 (1988).
[30]K. S. Fine, C. F. Driscoll, J. H. Malmberg, and T. B. Mitchell, "Measurements of symmetric vortex merger," Phys. Rev. Lett. **91**, 588 (1991).
[31]W. Matthaeus, W. T. Stribling, D. Martinez, S. Oughton, and D. Montgomery, "Selective decay and coherent vortices in two-dimensional turbulence," Phys. Rev. Lett. **66**, 2731 (1991).